

## Hessian-based Analysis of Large Batch Training and Robustness to Adversaries

ZHEWEI YAO<sup>1\*</sup>, AMIR GHOLAMI<sup>1\*</sup>, QI LEI<sup>2</sup>, KURT KEUTZER<sup>1</sup>, AND MICHAEL W. MAHONEY<sup>1</sup>

<sup>1</sup> University of California at Berkeley, {zheweyi, amirgh, keutzer, and mahoneymw}@berkeley.edu

<sup>2</sup> University of Texas at Austin, leiqi@ices.utexas.edu

**Abstract.** Large batch size training of Neural Networks has been shown to incur accuracy loss when trained with the current methods. The precise underlying reasons for this are still not completely understood. Here, we study large batch size training through the lens of the Hessian operator and robust optimization. In particular, we perform a Hessian based study to analyze how the landscape of the loss functional is different for large batch size training. We compute the true Hessian spectrum, without approximation, by back-propagating the second derivative. Our results on multiple networks show that, when training at large batch sizes, one tends to stop at points in the parameter space with noticeably higher/larger Hessian spectrum, i.e., where the eigenvalues of the Hessian are much larger. We then study how batch size affects robustness of the model in the face of adversarial attacks. All the results show that models trained with large batches are more susceptible to adversarial attacks, as compared to models trained with small batch sizes. Furthermore, we prove a theoretical result which shows that the problem of finding an adversarial perturbation is a saddle-free optimization problem. Finally, we show empirical results that demonstrate that adversarial training leads to areas with smaller Hessian spectrum. We present detailed experiments with five different network architectures tested on MNIST, CIFAR-10, and CIFAR-100 datasets.

**1. Introduction.** During the training of a Neural Network (NN), we are given a set of input data  $\mathbf{x}$  with the corresponding labels (or more generally response)  $y$  drawn from an unknown distribution  $\mathcal{P}$ . In practice, we only observe a set of discrete examples drawn from  $\mathcal{P}$ , and we want to train the Neural Network’s parameters to learn this unknown distribution. However, an open question is whether the training procedure actually leads to learning  $\mathcal{P}$ , or whether it is simply a smart/complicated way to overfit certain patterns in the dataset [26]? The seminal work of [13] showed that small perturbation in the input images, often imperceptible to human eyes, can easily fool the network. Some network architectures/models are known to be more robust than others (for instance RBF models [13] is robust). Here, we show that the robustness of a network is not only affected by the model’s architecture, but that training hyper-parameters can also significantly affect the robustness, relative to adversarial perturbations.

The standard optimization-based adversarial training procedure is to train the network on the original dataset until a desired accuracy is reached, and then solve a min-max optimization. This is commonly known as robust training in the optimization literature [3]. Here at each step we compute a perturbation which maximizes the value of the loss functional and then compute a descent direction on this example [13]. After several epochs of adversarial training, the network typically becomes more robust to these attacks. However, a fundamental question is: what exactly changes after the adversarial training that makes the network more robust? Also, why is the original model not robust to adversarial attacks to begin with?

We show that there is indeed a connection between the batch size used for training the model and its robustness to adversarial attacks. Large batch size training is known to suffer from low generalization performance as compared to small batches. This is a very fundamental issue, and there

---

\*Both authors contributed equally

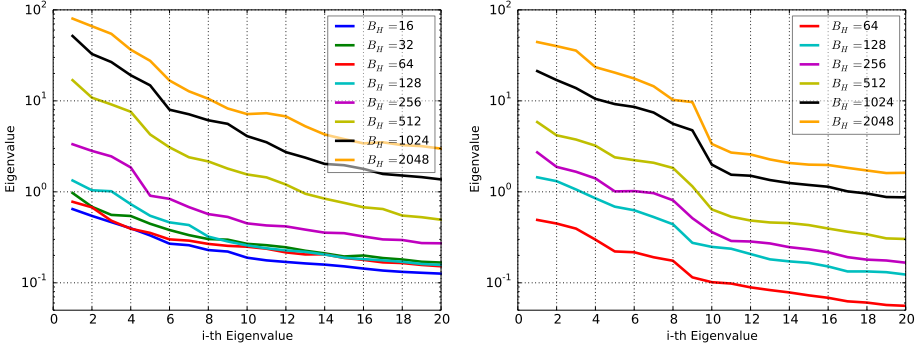


**Fig. 1:** Top 20 eigenvalues of the Hessian based on training dataset is shown for C1 network on CIFAR-10 (left) and M1 network on MNIST (right) datasets (please see Table 6 for details about the models). The spectrum is computed using power iteration with relative error of 1E-4. Observe that, for both models on different data sets, decreasing the batch size tends to lead to Hessian matrices (at the termination of training) that have smaller eigenvalues, i.e., smaller curvature around the solution.

have been numerous studies to understand this behavior. One proposed explanation is that large batch size training tends to get attracted to “sharp” minima [17]. Here, we perform a detailed analysis of this problem by studying the Hessian and find that there is actually a very interesting connection between large batch size training, robustness of the model, and adversarial training. Below are the details of the questions that we try to answer together with a brief summary of our answers:

**Q1** What is the difference between the local geometry of the neighborhood that the model converges to when large batch size is used as compared to small batch? In particular, how is the Hessian spectrum different? How does the loss functional change in a neighborhood of the solution for each case?

**A1:** We compute the spectrum of the true Hessian by back-propagating the second derivative. This follows [17], which used an approximate numerical method to compute the curvature of the model at a point. Our results show that large batch size training tends to stop at points with considerably “larger” Hessian spectrum.<sup>1</sup> For details please see §3.1. In short, please see Figs. 1, and 2, where we report the dominant eigenvalues for different batch sizes.

**Q2** How does the batch size affect the robustness of the model to adversarial perturbation? Equivalently, to what extent do different learned model parameters for the same architecture respond differently to adversarial perturbations?

**A2** We have observed that large batch size training is considerably more prone to adversarial attacks as compared to a model trained with small batch size. All the results tested on three different datasets with four different architectures show this behavior. Details are discussed in §3.2. In short, please see Tables 1 and 2 (along with Table 7 in the Appendix).

**Q3** Adversarial training can to some degree increase the network’s robustness to adversarial attack. How does the adversarial training affect the landscape of the objective functional in such a way that the trained network is more robust? Alternatively, why does the the original training not produce a

<sup>1</sup>By larger/higher we mean that the magnitude of the dominant eigenvalues is larger.

---

**Algorithm 1:** Adversarial training algorithm

---

**input** :  $N$  input images  $x$ , corresponding labels  $y$ ,  $m$  epochs,  $|B|$  mini-batch size, Neural Network model  $\mathcal{M}(\theta)$  with loss  $\mathcal{J}(\theta, \mathbf{x}, y)$ , hyper-parameter of iteration methods  $n, \epsilon$  magnitude of adversarial perturbation

**output** : Final model parameters  $\theta$

```
 $\theta = \arg \min \mathcal{J}(\theta, \mathbf{x}, y); \quad // \text{Initial Training}$ 
for  $i \leftarrow 1$  to  $mN/|B|$  do ;  $// \text{Adv. Training}$ 
  for  $i \leftarrow 1$  to  $n$  do ;  $// \text{Iterating Attack- n}$ 
     $\mathbf{x}^{\text{adv}} \leftarrow \mathbf{x} + \frac{1}{n} \Delta \mathbf{x} ; \quad // \text{Adv. Perturbation}$ 
     $\theta \leftarrow \theta - \eta \nabla_{\theta} \mathcal{J}(\theta, \mathbf{x}^{\text{adv}}, y)$ 
```

---

robust network?

**A3** We have empirically found that after adversarial training, the solution ends up at a point with noticeably smaller Hessian spectrum. We have also found a theoretical result which shows that the problem of solving for an adversarial perturbation is a saddle-free optimization problem with a low rank Hessian. The results are presented in §3.3. In short, please see Fig. 5, Fig. 11, Table 3, and Table 4.

**Limitations.** In this work, we have made an effort to avoid reporting only the best results. We have repeated all the experiments at least three times and found all the findings to be consistent. We showcase results on MNIST, CIFAR-10, and CIFAR-100. Given the size of the models, computing the whole spectrum of the Hessian is not a feasible task. Our spectrum computation is limited to the top 20 eigenvalues of the Hessian. We also prove that the Hessian of the loss w.r.t. the input is Positive Semidefinite. We note that this is only true for the assumptions that we have, which covers networks that strictly use ReLU activation (and in particular no batch norm layer).

**Related Work.** Deep Neural Networks have very good performance across a range of applications, most often when the optimization problem is solved with Stochastic Gradient Descent (SGD). The diversity of problems for which a DNN can be used has been related to their efficiency in function approximation [1, 7, 19, 25]. However, the work of [33] showed that not only the network can perform well on real dataset, but it can also memorize randomly labeled data very well. This should not be surprising, given by-now classical work on NN theory [23]. Moreover, the performance of the network is highly dependent on the hyper-parameters used for training. In particular, multiple recent studies have found that large batch size training suffers from poor generalization capability [14, 20, 32]. Recent studies also show that Neural Networks can easily be fooled by imperceptible perturbation to input data [13].

Here we focus on the latter two aspects of training Neural Networks. Prior work [17] presented results showing that large batches converge to “sharper minima”. Here, the argument is that even if the sharp minima have the same training loss as the flat ones, small discrepancies between the test data and the training data can easily lead to poor generalization performance [9, 17]. The fact

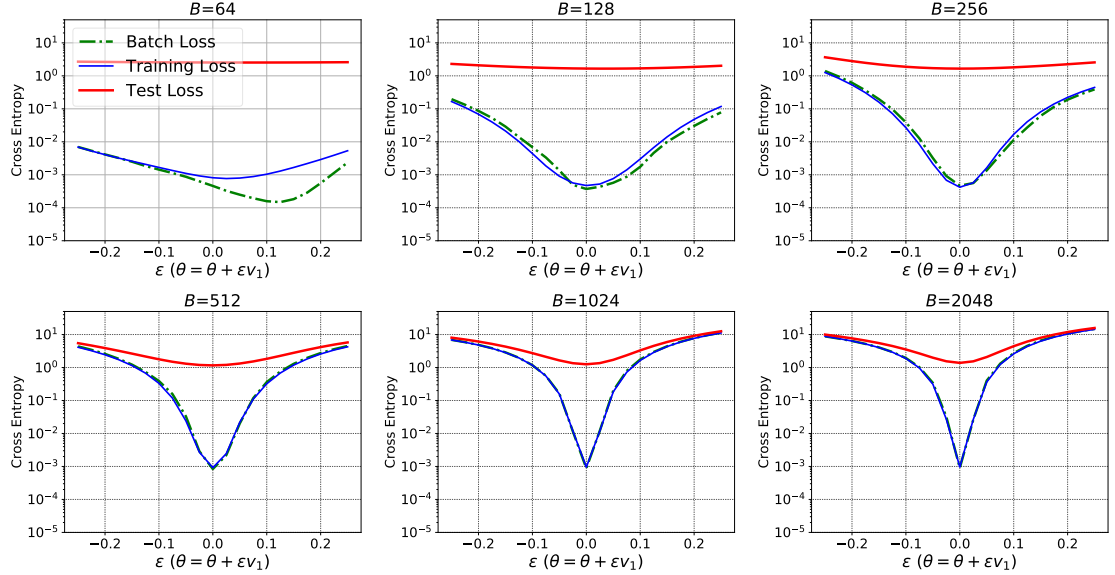


**Fig. 2:** The landscape of the loss functional ( $J(\theta, \mathbf{x}, \mathbf{y})$ ) is shown along the dominant eigenvector of the Hessian for C1 architecture on CIFAR-10 dataset (see Fig. 6 on for M1 on MNIST and Fig. 8 for C2 on CIFAR-10). Here  $\epsilon$  is a scalar that perturbs the model parameters along the dominant eigenvector denoted by  $v_1$ . The observation is that the curvature of test loss is much larger than that of training and batch loss when increasing training batch (note that the y-axis drawn on the logarithmic scale.). Also, notice that when the training batch is small (e.g. 64), batch and training loss have a large shift because the noise of a small batch is large.

that ‘‘flat minima’’ generalize well was also found earlier in [16]. The authors relate flat minima to the theory of minimum description length [27] and proposed an optimization method to favor flat minima. There have been several similar attempts to change the optimization algorithm to find ‘‘better’’ regions [6, 8]. For instance, [6] proposed entropy-SGD, which uses Langevin dynamics to augment the loss functional to favor flat regions of the ‘‘energy landscape’’. Importantly, the notion of flat/sharpness does not have an agreed-upon definition, and its informal use can lead to imprecision and confusion. A detailed comparison of different metrics is discussed in [9], where the authors show that sharp minima can also generalize well. In [29, 30], the authors proposed that the training can be viewed as a stochastic differential equation, and argued that the optimum batch size is proportional to the training size and the learning rate.

As our results show, there is an interleaved connection between robustness of the network and large batch size training. Prior work [13, 31] found that they can easily fool a NN with very good generalization by slightly perturbing the inputs. The perturbation magnitude is most of the time imperceptible to human eye, but it can completely change the network’s prediction. They introduced an effective adversarial attack algorithm known as Fast Gradient Sign Method (FGSM). They related the vulnerability of the Neural Network to linear classifiers and showed that RBF models, despite achieving much smaller generalization performance, are considerably more robust to FGSM attacks.

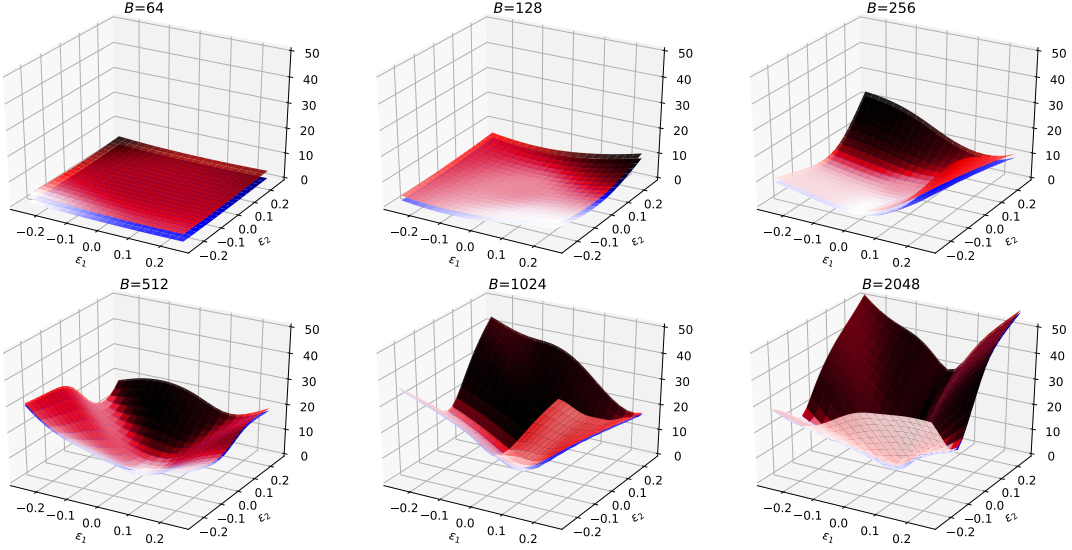


**Fig. 3:** The landscape of the loss functional is shown when the  $C1$  model parameters are changed along the first two dominant eigenvectors of the Hessian (see Fig. 7 on for  $M1$  on MNIST and Fig. 9 for  $C2$  on CIFAR-10). Here  $\epsilon_1, \epsilon_2$  are scalars that perturbs the model parameters along the first and second dominant eigenvectors. The blue (red) surface is for training (test) loss. Notice that the result of these plot is consistent with the that of Fig. 2, i.e. the curvature of test loss is much larger than that of training and batch loss when increasing training batch

The FGSM method was then extended in [18] to an iterative FGSM, which performs multiple gradient ascend steps to compute the adversarial perturbation. Adversarial attack based on iterative FGSM was found to be stronger than the original one step FGSM. Various defenses have been proposed to resist adversarial attacks [4, 11, 12, 15, 24]. However, recent work of [2] has shown that most of the defense methods can also be adversarially fooled. Understanding this goes back to the above problem, and the fact that we have not yet been able to fully understand how Neural Networks learn.

The structure of this paper is as follows: In section §2, we discuss details of how adversarial attack/training is performed. In particular, we provide theoretical proof that finding an adversarial perturbation is a saddle-free problem, under certain conditions of interest. Then, in section §3, we present our main empirical results: first, by fixing an attack method, and changing the batch size, as discussed in sections §3.1 and §3.2; and then, in section §3.3, by presenting results for how adversarial training changes the Hessian spectrum, for a fixed batch size. Finally, in section §4 we provide concluding remarks.

**2. Adversarial Attack.** The methods for adversarial attack on a Neural Network can broadly be split into white-box attacks, where the model architecture and its parameters are known, and black-box attacks, where such information is unavailable. Here we focus on the white-box methods, and in particular the optimization-based approach both for the attack and defense.

**Adversarial Attacks.** Suppose  $\mathcal{M}(\theta)$  is a learning model (the Neural Network architecture), and  $(\mathbf{x}, y)$  are the input data and the corresponding labels. The loss functional of the network with parameter  $\theta$  on  $(\mathbf{x}, y)$  is denoted by  $\mathcal{J}(\theta, \mathbf{x}, y)$ . For adversarial attack, we seek a perturbation  $\Delta\mathbf{x}$  (with a bounded  $L_\infty$  or  $L_2$  norm) such that it maximizes  $\mathcal{J}(\theta, \mathbf{x}, y)$ :

$$(2.1) \quad \max_{\|\Delta\mathbf{x}\| \in \mathcal{U}} \mathcal{J}(\theta, \mathbf{x} + \Delta\mathbf{x}, y),$$

where  $\mathcal{U}$  is an admissibility set for acceptable perturbation (typically restricting the magnitude of the perturbation). A typical choice for this set is  $\mathcal{U} = \mathbf{B}(\mathbf{x}, \epsilon)$ , a ball of radius  $\epsilon$  centered at  $\mathbf{x}$ . A popular method for approximately computing  $\Delta\mathbf{x}$  is Fast Gradient Sign Method [13], where the gradient of the loss functional is computed w.r.t. inputs, and the perturbation is set to:

$$(2.2) \quad \Delta\mathbf{x} = \epsilon \operatorname{sign}\left(\frac{\partial \mathcal{J}(\mathbf{x}, \theta)}{\partial \mathbf{x}}\right).$$

This is not the only attack method possible. Other approaches include an iterative FGSM method (FGSM-10)[18] or using other norms such as  $L_2$  norm instead of  $L_\infty$  (We denote the  $L_2$  method by  $L_2GRAD$  in our results). Here we also use a second-order attack, i.e., going beyond just the gradient to include Hessian-based information in the attack method. We use the Hessian w.r.t. input to precondition the gradient direction with second order information (Algorithm 1). Similar to the gradient methods, we denote FHSM ( $L_2HESS$ ) when we use  $L_\infty$  ( $L_2$ ) norm for the admissibility set. Please see Table 5 for more details.

**Adversarial Defenses.** Now one method to defend against such adversarial attacks, is to perform robust training [21, 31]:

$$(2.3) \quad \min_{\theta} \max_{\|\Delta\mathbf{x}\| \in \mathcal{U}} \mathcal{J}(\theta, \mathbf{x} + \Delta\mathbf{x}, y),$$

as shown in Algorithm 1.

Solving this min-max optimization problem at each iteration requires first finding the worst adversarial perturbation that maximizes the loss functional, and then updating the model parameters  $\theta$  with the perturbed inputs. Since adversarial examples have to be generated at every iteration, it would not be feasible to find the exact perturbation that maximizes the objective functional. Instead, a popular method is to perform single or multiple gradient ascents to compute  $\Delta\mathbf{x}$  approximately. After approximating  $\Delta\mathbf{x}$  at each iteration, a typical optimization step (variant of SGD) is performed to update  $\theta$ .

**Adversarial Perturbation as a Saddle-free Problem.** Here we show that solving the maximization part is actually a saddle-free problem *almost everywhere*. Recall that our loss functional is  $\mathcal{J}(\theta; \mathbf{x}, y)$ . We make following assumptions for the model to help show our theoretical result,

ASSUMPTION 1. *We assume the model's activation functions are strictly ReLU activations, and all layers are either convolution or fully connected. Note that even though the ReLU activation has discontinuity at the origin, i.e., at  $x = 0$ , the ReLU function is twice differentiable almost everywhere.*

The following theorem shows that, in this special case, the problem of finding an adversarial perturbation that maximizes  $\mathcal{J}$  is a saddle-free optimization problem, with a Positive Semidefinite Hessian w.r.t. input almost everywhere. For details on the proof please see Appendix. A.1.

**THEOREM 2.1.** *With Assumption. 1, for a DNN, its loss functional  $\mathcal{J}(\theta, \mathbf{x}, y)$  is a saddle-free function w.r.t. input  $\mathbf{x}$  almost everywhere, i.e.,*

$$\frac{\partial^2 \mathcal{J}(\theta, \mathbf{x}, y)}{\partial \mathbf{x}^2} \succeq 0.$$

From the proof of Theorem 2.1, we immediately get the following proposition with respect to DNNs; see Appendix A.1 for more details on this result.

**PROPOSITION 2.2.** *Based on Theorem 2.1 with Assumption 1, if the input  $\mathbf{x} \in \mathbb{R}^d$  and the number of the output class is  $c$ , i.e.,  $y \in \{1, 2, 3, \dots, c\}$ , then the Hessian of DNNs w.r.t. to  $\mathbf{x}$  is at most a rank  $c$  matrix almost everywhere.*

**3. Main Results.** In this section, we will present numerical experiments to analyze large batch size training, its robustness to adversarial attacks, and how adversarial training changes the model.

**3.1. Large Batch and Hessian Spectrum. Setup:** The architecture for the networks used is reported in the appendix (please see Table 6). In the text, we refer to each architecture by the abbreviation used in this table. Unless otherwise specified, each of the batch sizes are trained until a training loss of 0.001 or better is achieved. Different batches are trained with the same starting learning rate and same momentum, and no weight decay is used.

We first focus on large batch size training versus small batch and report the results for large batch training for C1 network on CIFAR-10 dataset are shown in Table 1 (and Table 7 for M1 model on MNIST). As one can see, after a certain point increasing batch size results in performance degradation on the test dataset (please see the Acc. (second) column). This is in line with results in the literature [14, 17].

As discussed before, one popular argument about large batch size's poor generalization accuracy has been that large batches tend to get attracted to "sharp" minima of the training loss. In [17] an approximate  $\epsilon$  – sharpness metric was used to measure curvature of the loss function for a given model parameter. Here, we directly compute the Hessian spectrum. Note that computing the whole Hessian matrix is infeasible as it is a  $\mathcal{O}(N^2)$  matrix. However, the spectrum can be computed using power iteration by back-propagating the matvec of the Hessian [22]. Unless otherwise noted, we continue the power iterations until a relative error of 1E-4 reached for each individual eigenvalue.

With this approach, we have computed the top 20 eigenvalues of the Hessian for different batch sizes as shown in Fig. 1. Moreover, the dominant eigenvalue, denoted by  $\lambda_1^\theta$  is also reported in Table 1, and Table 2, respectively.<sup>2</sup> From Fig. 1, we can clearly see that for all the experiments, large batches have a noticeably larger Hessian spectrum both in the dominant eigenvalue as well as the rest of the 19 eigenvalues. But note that curvature is a very local measure. It would be more informative to

---

<sup>2</sup>Additional result for MNIST tested using LeNet-5 is given in appendix. Please see Table 7.

**Table 1:** Result on CIFAR-10 dataset using C1, C2 network (see Table 7 for M1 on MNIST). We show the Hessian spectrum of different batch training models, and the corresponding performances on adversarial dataset generated by training/testing dataset. Results for the testing dataset are given in parenthesis. We report the adversarial accuracy of three different magnitudes of attack. The interesting observation is that the  $\lambda_1^\theta$  is increasing while the adversarial accuracy is decreasing for fixed  $\epsilon$ . Also, notice that it seems no correlation between  $\lambda_1^\theta$ ,  $\|\nabla_{\mathbf{x}}\mathcal{J}\|$  and the adversarial accuracy.

Batch	Acc.	$\lambda_1^\theta$	$\lambda_1^\mathbf{x}$	$\ \nabla_{\mathbf{x}}\mathcal{J}\ $	Acc $\epsilon = 0.02$	Acc $\epsilon = 0.01$	Acc $\epsilon = 0.005$
C1 Cifar-10	16	100 (77.68)	0.64 (32.78)	2.69 (200.7)	0.05 (20.41)	48.07 (30.38)	72.67 (42.70)
	32	100 (76.77)	0.97 (45.28)	3.43 (234.5)	0.05 (23.55)	49.04 (31.23)	72.63 (43.30)
	64	100 (77.32)	0.77 (48.06)	3.14 (195.0)	0.04 (21.47)	50.40 (32.59)	73.85 (44.76)
	128	100 (78.84)	1.33 (137.5)	1.41 (128.1)	0.02 (13.98)	33.15 (25.2 )	57.69 (39.09)
	256	100 (78.54)	3.34 (338.3)	1.51 (132.4)	0.02 (14.08)	25.33 (19.99)	50.10 (34.94)
	512	100 (79.25)	16.88 (885.6)	1.97 (100.0)	0.04 (10.42)	14.17 (12.94)	28.54 (25.08)
	1024	100 (78.50)	51.67 (2372 )	3.11 (146.9)	0.05 (13.33)	8.80 (8.40 )	23.99 (21.57)
	2048	100 (77.31)	80.18 (3769 )	5.18 (240.2)	0.06 (18.08)	4.14 (3.77 )	17.42 (16.31)
C2 Cifar-10	256	100 (79.20)	0.62 (28 )	12.10 (704.0)	0.10 (41.95)	0.57 (0.38)	0.73 (0.47)
	512	100 (80.44)	0.75 (57 )	4.82 (425.2)	0.03 (26.14)	0.34 (0.25)	0.54 (0.38)
	1024	100 (79.61)	2.36 (142)	0.523 (229.9)	0.04 (17.16)	0.27 (0.22)	0.46 (0.35)
	2048	100 (78.99)	4.30 (307)	0.145 (260.0)	0.50 (17.94)	0.18 (0.16)	0.33 (0.28)
C2							

**Table 2:** Result on CIFAR-100 dataset using CR network. We show the Hessian spectrum of different batch training models, and the corresponding performances on adversarial dataset generated by training/testing dataset. Results for the testing dataset is given in parenthesis. We report the adversarial accuracy of three different magnitudes of attack. All models are trained until a total loss less than 0.02 is achieved. The interesting observation is that the  $\lambda_1^\theta$  is increasing while the adversarial accuracy is decreasing for fixed  $\epsilon$ .

Batch	Acc.	$\lambda_1^\theta$	Acc $\epsilon = 0.02$	Acc $\epsilon = 0.01$	Acc $\epsilon = 0.005$
64	99.98 (70.81)	0.022 (10.43)	61.54 (34.48)	78.57 (39.94)	96.88 (49.43)
128	99.97 (70.9 )	0.055 (26.50 )	58.15 (33.73)	77.41 (38.77)	97.01 (48.67)
256	99.98 (68.6 )	1.090 (148.29)	39.96 (28.37)	66.12 (35.02)	94.11 (47.17)
512	99.98 (68.6 )	1.090 (148.29)	40.48 (28.37)	66.09 (35.02)	94.06 (47.17)

study how the loss behaves in a neighborhood around the point to which the model has converged. To visually demonstrate this, we have plotted how the total loss functional changes when the model parameters are perturbed along the dominant eigenvector as shown in Fig. 2, and Fig. 6 for C1 and M1 models, respectively. We can clearly see that the large batch size models have been attracted to areas with higher curvature for both the test and training losses.

We have also added a 3D plot, where we perturb the parameters of C1 model along both the first and second eigenvectors as shown in Fig. 3. The visual results are in line with the numbers shown for the Hessian spectrum (see  $\lambda_1^\theta$ ) in Table 1, and Table 7. For instance, note the value of  $\lambda_1^\theta$  for the training and test loss for  $B = 2048, 512$  and compare the corresponding results in Fig. 3.

**3.2. Large Batch and Adversarial Attack.** Here, we test the robustness of the models trained with different batches to an adversarial attack. We use the Fast Gradient Sign Method for all the experiments (we did not see any difference in the conclusions with FGSM-10 attack). The adversarial performance is measured by the fraction of correctly classified adversarial inputs. We report the performance for both the training and test datasets for different values of  $\epsilon = 0.02, 0.01$ , and  $0.005$  ( $\epsilon$  is the metric for the adversarial perturbation magnitude). The performance results for C1, and C2 models on CIFAR-10, along with a resnet model (CR) on CIFAR-100, are reported in the last three columns of Tables 1 and 2 (MNIST results are given in appendix Table 7). The interesting observation is that for all the cases, large batches are considerably more prone to adversarial attacks as compared to small batches (see the last three columns). This means that not only the network design affects the robustness of the model, but also the hyper-parameters used during optimization, and in particular where in the parameter space ( $\theta$ ) the model has converged to.

**Table 3:** Accuracy of different models across different adversarial samples of M1 on MNIST test dataset, which are obtained by perturbing the original model  $\mathcal{M}_{ORI}$  (see Table 4 for C3 on CIFAR-10). See that after adversarial training the model becomes more robust to all attacks. Also note that the accuracy of different adversarial attacks varies.

	$\mathcal{D}_{clean}$	$\mathcal{D}_{FGSM}$	$\mathcal{D}_{FGSM10}$	$\mathcal{D}_{L_2GRAD}$	$\mathcal{D}_{FHSM}$	$\mathcal{D}_{L_2HESS}$	MEAN of Adv
$\mathcal{M}_{ORI}$	99.32	60.37	77.27	14.32	82.04	33.21	53.44
$\mathcal{M}_{FGSM}$	99.49	96.18	97.44	63.46	97.56	83.33	87.59
$\mathcal{M}_{FGSM10}$	<b>99.5</b>	96.52	<b>97.63</b>	66.15	97.66	84.64	88.52
$\mathcal{M}_{L_2GRAD}$	98.91	<b>96.88</b>	97.39	<b>86.23</b>	<b>97.66</b>	<b>92.56</b>	<b>94.14</b>
$\mathcal{M}_{FHSM}$	99.45	94.41	96.48	52.67	96.89	77.58	83.60
$\mathcal{M}_{L_2HESS}$	98.72	95.02	96.49	77.18	97.43	90.33	91.29

As a potential explanation for why large batches are more susceptible to adversarial attacks we have analyzed the gradient and Hessian w.r.t.  $\mathbf{x}$  (hereafter referred to as input Hessian). We have computed the dominant eigenvalue of this input Hessian using power iteration for each individual input sample from both the training and testing datasets. Furthermore, we have computed the norm of the gradient w.r.t.  $\mathbf{x}$  for these datasets as well. These two metrics are denoted by  $\lambda_1^{\mathbf{x}} = \frac{1}{N} \sum_{i=1}^N \left\| \frac{\partial^2 \mathcal{J}(\theta, \mathbf{x}_i)}{\partial \mathbf{x}_i^2} \right\|$ , and  $\|\nabla_{\mathbf{x}} \mathcal{J}\| = \frac{1}{N} \sum_{i=1}^N \left\| \frac{\partial \mathcal{J}(\theta, \mathbf{x}_i)}{\partial \mathbf{x}} \right\|$ . The results on all of our experiments show that these two metrics do not correlate with the adversarial accuracy. For instance, consider C1 model with  $B = 512$ . It has both smaller gradient and smaller input Hessian eigenvalue as compared to  $B = 32$ , but it performs noticeably worse under adversarial attack. One possible conjecture could be that the decision boundaries of the network for large batches are less stable, such that with small adversarial perturbation the model gets fooled. It seems this notion of stability is not directly correlated with input Hessian and input gradient.

**3.3. Adversarial Training and Hessian Spectrum.** In this part, we study how the Hessian spectrum and the landscape of the loss change after adversarial training. Here, we fix the batch size (and all other optimization hyper-parameters) and use five different adversarial training methods as described in §2.

**Table 4:** Accuracy of different models across different samples of  $C3$  on CIFAR-10 test dataset, which are obtained by perturbing the original model  $\mathcal{M}_{ORI}$ . Observe that after adversarial training the model becomes more robust to all attacks. Also notice that the accuracy of different adversarial attacks varies.

	$\mathcal{D}_{clean}$	$\mathcal{D}_{FGSM}$	$\mathcal{D}_{FGSM10}$	$\mathcal{D}_{L_2GRAD}$	$\mathcal{D}_{FHSM}$	$\mathcal{D}_{L_2HESS}$	MEAN of Adv
$\mathcal{M}_{ORI}$	<b>79.46</b>	15.25	4.46	12.37	29.64	22.93	16.93
$\mathcal{M}_{FGSM}$	71.82	63.05	63.44	57.68	<b>66.04</b>	62.36	62.51
$\mathcal{M}_{FGSM10}$	71.14	<b>63.32</b>	<b>63.88</b>	<b>58.25</b>	65.95	<b>62.70</b>	<b>62.82</b>
$\mathcal{M}_{L_2GRAD}$	63.52	59.33	59.73	57.35	60.44	58.98	59.16
$\mathcal{M}_{FHSM}$	74.34	47.65	43.95	38.45	62.75	55.77	49.71
$\mathcal{M}_{L_2HESS}$	71.59	50.05	46.66	42.95	62.87	58.42	52.19

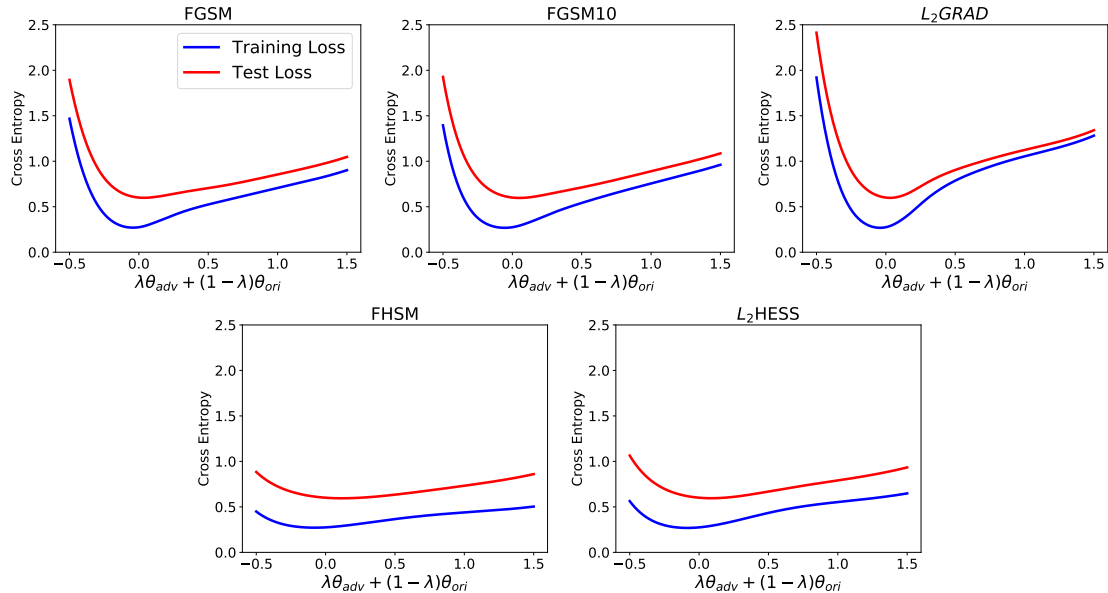


**Fig. 4:** 1-D Parametric plot for  $C3$  model on CIFAR-10 dataset (see Fig. 10 for  $M1$  on MNIST). We interpolate between weight parameters of  $\mathcal{M}_{ORI}$  and  $\mathcal{M}_{ADV}$ , and compute the cross entropy loss on the  $y$ -axis. Notice the robust models are at a point that has smaller curvature as compared to the original model.

For the sake of clarity, let us denote  $\mathcal{D}$  to be the test dataset, which can be the original clean test dataset or one created by using an adversarial method. For instance, we denote  $\mathcal{D}_{FGSM}$  to be the adversarial dataset generated by FGSM, and  $\mathcal{D}_{clean}$  to be the original clean test dataset.

**Setup.** For the MNIST experiments, we train a standard LeNet on MNIST dataset (using M1 network). For the original training, we set the learning rate to 0.01 and momentum to 0.9, and decay the learning rate by half after every 5 epochs, for a total of 100 epochs. Then we perform an additional five epochs of adversarial training with a learning rate of 0.01. The perturbation magnitude,  $\epsilon$ , is set to 0.1. We also present results for C3 model [5] on CIFAR-10, using the same hyper-parameters,

except that the training is performed for 100 epochs. Afterwards, adversarial training is performed for a subsequent 10 epochs with a learning rate of 0.01 and momentum of 0.9. The learning rate is decayed by half after every five epochs. Furthermore, the adversarial perturbation magnitude is set to  $\epsilon = 0.02$  [28].

The results are shown in Table 3, and Table 4. We can see that after adversarial training the model becomes more robust to these attacks. Note that the accuracy of different adversarial attacks varies. In addition, all adversarial training methods improve the robustness relative to the adversarial dataset, though they reduce accuracy on  $\mathcal{D}_{clean}$ , which is consistent with the observations in [13]. As an example, consider the second row of Table 3 which shows the results when FGSM. The performance of this model when tested against the  $L_2GRAD$  attack method is 63.46% as opposed to 14.32% of the original model ( $\mathcal{M}_{ORI}$ ). The rest of the rows show the results for different algorithms.

The main question here is how does the landscape of the loss functional change after these robust optimizations are performed? We first show a 1-D parametric interpolation between the original model parameters  $\theta$  and that of the robustified models, as shown in Fig. 4 (please see Fig. 10 for MNIST). Notice the robust models are at a point that has smaller curvature as compared to the original model. To exactly quantify this, we compute the spectrum of the Hessian as shown in Fig. 5 (and Fig. 11 for MNIST). Besides the full Hessian spectrum, we also report the spectrum of sub-sampled Hessian. The latter is computed by randomly selecting a subset of the training dataset. We denote the size of this subset as  $B_H$  to avoid confusion with the training batch size. In particular, we report results for  $B_H = 1$  and  $B_H = 320$ . There are several important observations here. First, notice that the spectrum of the robust models is noticeably smaller than the original model. Second, note that even though the total Hessian shows that we have converged to a point with positive curvature (at least based on the top 20 eigenvalues), but that is not necessarily the case when we look at individual samples (i.e.  $B_H = 1$ ). For a randomly selected batch of  $B_H = 1$ , we see that we have actually converged to a point that has both positive and negative curvatures. This is because SGD optimizes the expected loss instead of individual ones.

**3.4. Discussion on Second Order Method.** Although second order adversarial attack looks well for MNIST (see Table 3), for most our experiments on CIFAR-10 (see Table 4), the second order methods are weaker than variations of the gradient based methods. Also, notice that the robust models trained by second order method are also more prone to attack on CIFAR-10, particularly  $\mathcal{M}_{FHSM}$  and  $\mathcal{M}_{L_2HESS}$ . We give two potential explanation here.

First note that based on Proposition 2.2, the Hessian w.r.t. input is a low rank matrix. In fact, the rank of the input Hessian for CIFAR-10/MNIST is at most ten, even though the matrix itself is  $3K \times 3K$ . We used inexact Newton method [10] along with Conjugate Gradient solver to apply the inverse Hessian operator, but this low rank nature can still create numerical problems. Addressing this issue requires designing preconditioners for second-order attacks, which is part of our future work. The second conjecture is that, as we saw in the previous section, the input Hessian does not directly correlate with how robust the network is. Intuitively, the most effective attack method should be one that perturbs the input towards the decision boundary which is not well captured by

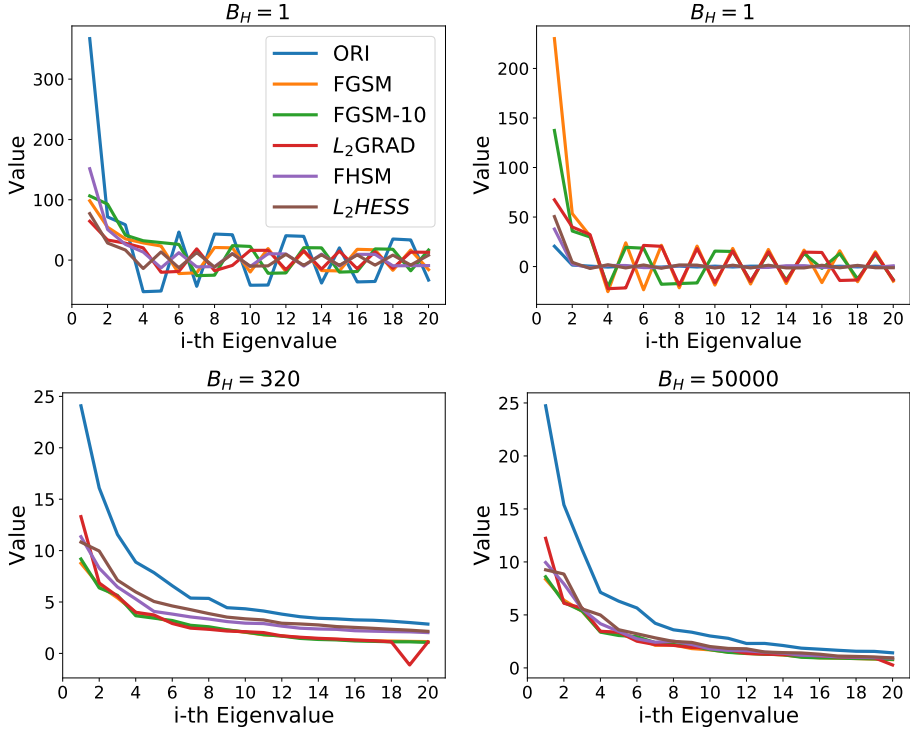


**Fig. 5:** Spectrum of the sub-sampled Hessian of the loss functional w.r.t. the model parameters for C3 on CIFAR-10 dataset (see Fig. 11 for M1 on MNIST). The results are computed for different batch sizes of  $B_H = 1$  (two cases),  $B_H = 320$ , and  $B_H = 50000$ . The samples of  $B_H = 1, 320$  are randomly chosen from training dataset. First, notice that the spectrum of the robust models is noticeably smaller than the original model. Second, note that even though the total Hessian shows the top 20 eigenvalues are positive, but that is not true of  $B_H = 1$ .

an unpreconditioned second order attack.

**4. Conclusion.** In this work, we studied Neural Networks through the lens of the Hessian operator. In particular, we studied the impact of large batch size training on the stability of the model in the presence of white-box adversarial attacks. We computed the matvec of the Hessian operator and computed its spectrum using power iteration. We provided several evidences that show that large batch size training tends to get attracted to areas with higher Hessian spectrum. We reported the top 20 eigenvalues of the Hessian, computed on all of the dataset samples, and we plotted the landscape of the loss when perturbed along the dominant Hessian eigenvector. Visual results were in line with the numerical values for the spectrum. We showed that, although the model converges to an area with positive curvature when considering all of the training dataset (i.e., total loss), if we look at individual samples then the Hessian can actually have significant negative eigenvalues. From an optimization viewpoint, this is due to the fact that SGD optimizes the expected loss and not the individual per sample loss.

Our empirical results show that adversarial attacks/training and large batches are closely related. We provided several empirical results on multiple datasets that show large batch size training is more prone to adversarial attacks. This means that not only the model design is important, but also the optimization hyper-parameters can drastically affect a network’s stability. Furthermore, we observed that, after robust training, the model’s parameters are at a point with noticeably smaller Hessian spectrum w.r.t.  $\theta$ .

The results show that the robustness of the model does not (at least directly) correlate with the Hessian w.r.t.  $\mathbf{x}$ . We also found that this Hessian is actually a Positive Semidefinite matrix, meaning that the problem of finding the adversarial perturbation is actually a saddle-free problem for cases that satisfy assumption 1.

## References.

- [1] Martin Anthony and Peter L Bartlett. *Neural network learning: Theoretical foundations*. cambridge university press, 2009.
- [2] Anish Athalye, Nicholas Carlini, and David Wagner. “Obfuscated gradients give a false sense of security: Circumventing defenses to adversarial examples”. In: *arXiv preprint arXiv:1802.00420* (2018).
- [3] A. Ben-Tal, L. El Ghaoui, and A.S. Nemirovski. *Robust Optimization*. Princeton Series in Applied Mathematics. Princeton University Press, 2009.
- [4] Arjun Nitin Bhagoji, Daniel Cullina, and Prateek Mittal. “Dimensionality reduction as a defense against evasion attacks on machine learning classifiers”. In: *arXiv preprint arXiv:1704.02654* (2017).
- [5] Nicholas Carlini and David Wagner. “Towards evaluating the robustness of Neural Networks”. In: *Security and Privacy (SP)*. IEEE. 2017, pp. 39–57.
- [6] Pratik Chaudhari, Anna Choromanska, Stefano Soatto, and Yann LeCun. “Entropy-SGD: Biassing gradient descent into wide valleys”. In: *arXiv preprint arXiv:1611.01838* (2016).
- [7] Olivier Delalleau and Yoshua Bengio. “Shallow vs. deep sum-product networks”. In: *Advances in Neural Information Processing Systems*. 2011, pp. 666–674.
- [8] Guillaume Desjardins, Karen Simonyan, Razvan Pascanu, and Koray Kavukcuoglu. “Natural neural networks”. In: *Advances in Neural Information Processing Systems*. 2015, pp. 2071–2079.
- [9] Laurent Dinh, Razvan Pascanu, Samy Bengio, and Yoshua Bengio. “Sharp minima can generalize for deep nets”. In: *arXiv preprint arXiv:1703.04933* (2017).
- [10] Stanley C Eisenstat and Homer F Walker. “Choosing the forcing terms in an inexact Newton method”. In: *SIAM Journal on Scientific Computing* 17.1 (1996), pp. 16–32.
- [11] Reuben Feinman, Ryan R Curtin, Saurabh Shintre, and Andrew B Gardner. “Detecting adversarial samples from artifacts”. In: *arXiv preprint arXiv:1703.00410* (2017).
- [12] Zhitao Gong, Wenlu Wang, and Wei-Shinn Ku. “Adversarial and clean data are not twins”. In: *arXiv preprint arXiv:1704.04960* (2017).
- [13] Ian J Goodfellow, Jonathon Shlens, and Christian Szegedy. “Explaining and harnessing adversarial examples”. In: *arXiv preprint arXiv:1412.6572* (2014).

[14] Priya Goyal, Piotr Dollár, Ross Girshick, Pieter Noordhuis, Lukasz Wesolowski, Aapo Kyrola, Andrew Tulloch, Yangqing Jia, and Kaiming He. “Accurate, large minibatch SGD: training imagenet in 1 hour”. In: *arXiv preprint arXiv:1706.02677* (2017).

[15] Kathrin Grosse, Praveen Manoharan, Nicolas Papernot, Michael Backes, and Patrick McDaniel. “On the (statistical) detection of adversarial examples”. In: *arXiv preprint arXiv:1702.06280* (2017).

[16] Sepp Hochreiter and Jürgen Schmidhuber. “Flat minima”. In: *Neural Computation* 9.1 (1997), pp. 1–42.

[17] Nitish Shirish Keskar, Dheevatsa Mudigere, Jorge Nocedal, Mikhail Smelyanskiy, and Ping Tak Peter Tang. “On large-batch training for deep learning: Generalization gap and sharp minima”. In: *arXiv preprint arXiv:1609.04836* (2016).

[18] Alexey Kurakin, Ian Goodfellow, and Samy Bengio. “Adversarial examples in the physical world”. In: *arXiv preprint arXiv:1607.02533* (2016).

[19] Nicolas Le Roux and Yoshua Bengio. “Deep belief networks are compact universal approximators”. In: *Neural computation* 22.8 (2010), pp. 2192–2207.

[20] Yann LeCun, Léon Bottou, Genevieve B Orr, and Klaus-Robert Müller. “Efficient backprop”. In: *Neural networks: Tricks of the trade* (1998), pp. 9–50.

[21] Aleksander Madry, Aleksandar Makelov, Ludwig Schmidt, Dimitris Tsipras, and Adrian Vladu. “Towards deep learning models resistant to adversarial attacks”. In: *International Conference on Learning Representations* (2018). URL: <https://openreview.net/forum?id=rJzIBfZAb>.

[22] James Martens and Ilya Sutskever. “Training deep and recurrent networks with Hessian-free optimization”. In: *Neural Networks: Tricks of the trade*. Springer, 2012, pp. 479–535.

[23] Charles H Martin and Michael W Mahoney. “Rethinking generalization requires revisiting old ideas: statistical mechanics approaches and complex learning behavior”. In: *arXiv preprint arXiv:1710.09553* (2017).

[24] Jan Hendrik Metzen, Tim Genewein, Volker Fischer, and Bastian Bischoff. “On detecting adversarial perturbations”. In: *arXiv preprint arXiv:1702.04267* (2017).

[25] Guido F Montufar, Razvan Pascanu, Kyunghyun Cho, and Yoshua Bengio. “On the number of linear regions of deep neural networks”. In: *Advances in neural information processing systems*. 2014, pp. 2924–2932.

[26] Nicolas Papernot, Nicholas Carlini, Ian Goodfellow, Reuben Feinman, Fartash Faghri, Alexander Matyasko, Karen Hambardzumyan, Yi-Lin Juang, Alexey Kurakin, Ryan Sheatsley, et al. “cleverhans v2. 0.0: an adversarial machine learning library”. In: *arXiv preprint arXiv:1610.00768* (2016).

[27] Jorma Rissanen. “Modeling by shortest data description”. In: *Automatica* 14.5 (1978), pp. 465–471.

[28] Uri Shaham, Yutaro Yamada, and Sahand Negahban. “Understanding adversarial training: Increasing local stability of Neural Nets through robust optimization”. In: *arXiv preprint arXiv:1511.05432* (2015).

- [29] Samuel L Smith, Pieter-Jan Kindermans, and Quoc V Le. “Don’t decay the learning rate, increase the batch size”. In: *arXiv preprint arXiv:1711.00489* (2017).
- [30] Samuel L Smith and Quoc V Le. “A Bayesian perspective on generalization and stochastic gradient descent”. In: *Second workshop on Bayesian Deep Learning (NIPS 2017)* (2017).
- [31] Christian Szegedy, Wojciech Zaremba, Ilya Sutskever, Joan Bruna, Dumitru Erhan, Ian Goodfellow, and Rob Fergus. “Intriguing properties of neural networks”. In: *arXiv preprint arXiv:1312.6199* (2013).
- [32] Yang You, Igor Gitman, and Boris Ginsburg. “Scaling SGD batch size to 32K for ImageNet training”. In: *arXiv preprint arXiv:1708.03888* (2017).
- [33] Chiyuan Zhang, Samy Bengio, Moritz Hardt, Benjamin Recht, and Oriol Vinyals. “Understanding deep learning requires rethinking generalization”. In: *arXiv preprint arXiv:1611.03530* (2016).

## Appendix A. Appendix.

**A.1. Proof of Theorem 1.** In this section, we give the proof of Theorem 2.1. The first thing we want to point out is that, although we prove the Hessians of these NNs are positive semi-definite almost everywhere, these NNs are not convex w.r.t. inputs, i.e.,  $\mathbf{x}$ . The discontinuity of ReLU is the cause. (For instance, consider a combination of two step functions in 1-D, e.g.  $f(x) = 1_{x \geq 1} + 1_{x \geq 2}$  is not a convex function but has 0 second derivative almost everywhere.) However, this has an important implication, that the problem is saddle-free.

Before we go to the proof of Theorem 2.1, let us prove the following lemma for cross-entropy loss with soft-max layer.

LEMMA A.1. *Let us denote by  $\mathbf{s} \in \mathbb{R}^d$  the input of the soft-max function, by  $y \in \{1, 2, \dots, d\}$  the correct label of the inputs  $\mathbf{x}$ , by  $g(\mathbf{s})$  the soft-max function, and by  $L(\mathbf{s}, y)$  the cross-entropy loss. Then we have*

$$\frac{\partial^2 L(\mathbf{s}, y)}{\partial \mathbf{s}^2} \succeq \mathbf{0}.$$

*Proof.* Let  $s_d = \sum_{j=1}^d e^{\mathbf{s}_j}$ ,  $\mathbf{p}_i = \frac{e^{\mathbf{s}_i}}{s_d}$ , and then it follows that

$$L(\mathbf{s}, y) = - \sum_{i=1}^d y_i \log \mathbf{p}_i.$$

Further, it is not hard to see that

$$\begin{aligned} \frac{\partial L(\mathbf{s}, y)}{\partial \mathbf{s}_j} &= - \sum_{i=1}^d y_i \frac{\partial \log \mathbf{p}_i}{\partial \mathbf{s}_j} \\ &= -y_j(1 - \mathbf{p}_j) - \sum_{i \neq j} y_i \frac{\mathbf{p}_k \mathbf{p}_j}{\mathbf{p}_k} \\ &= \mathbf{p}_j - y_j. \end{aligned}$$

Then, the second order derivative of  $L$  w.r.t.  $\mathbf{s}_i \mathbf{s}_j$  is

$$\frac{\partial^2 L(\mathbf{s}, y)}{\partial \mathbf{s}_j^2} = \mathbf{p}_j(1 - \mathbf{p}_j), \quad \text{and} \quad \frac{\partial^2 L(\mathbf{s}, y)}{\partial \mathbf{s}_j \partial \mathbf{s}_i} = -\mathbf{p}_j \mathbf{p}_i.$$

Since

$$\frac{\partial^2 L(\mathbf{s}, y)}{\partial \mathbf{s}_j^2} + \sum_{i \neq j} \frac{\partial^2 L(\mathbf{s}, y)}{\partial \mathbf{s}_j \partial \mathbf{s}_i} = 0, \quad \text{and} \quad \frac{\partial^2 L(\mathbf{s}, y)}{\partial \mathbf{s}_j^2} \geq 0,$$

we have

$$\frac{\partial^2 L(\mathbf{s}, y)}{\partial \mathbf{s}^2} \succeq \mathbf{0}.$$

□

Now, let us give the proof of Theorem 2.1:

Assume the input of the soft-max layer is  $\mathbf{s}$  and the cross-entropy is  $L(\mathbf{s}, y)$ . Based on Chain Rule, it follows that

$$\frac{\partial \mathcal{J}(\boldsymbol{\theta}, \mathbf{x}, y)}{\partial \mathbf{x}} = \frac{\partial L}{\partial \mathbf{s}} \frac{\partial \mathbf{s}}{\partial \mathbf{x}}.$$

From Assumption. 1 we know that all the layers before the soft-max are either linear or ReLU, which indicates  $\frac{\partial^2 \mathbf{s}}{\partial \mathbf{x}^2} = \mathbf{0}$  (a tensor) almost everywhere. Therefore, applying chain rule again for the above equation,

$$\begin{aligned}\frac{\partial^2 \mathcal{J}(\boldsymbol{\theta}, \mathbf{x}, y)}{\partial \mathbf{x}^2} &= \left(\frac{\partial \mathbf{s}}{\partial \mathbf{x}}\right)^T \frac{\partial^2 L}{\partial \mathbf{s}^2} \frac{\partial \mathbf{s}}{\partial \mathbf{x}} + \frac{\partial L}{\partial \mathbf{s}} \frac{\partial^2 \mathbf{s}}{\partial \mathbf{x}^2} \\ &= \left(\frac{\partial \mathbf{s}}{\partial \mathbf{x}}\right)^T \frac{\partial^2 L}{\partial \mathbf{s}^2} \frac{\partial \mathbf{s}}{\partial \mathbf{x}}.\end{aligned}$$

It is easy to see  $\frac{\partial^2 \mathcal{J}(\boldsymbol{\theta}, \mathbf{x}, y)}{\partial \mathbf{x}^2} \succeq 0$  almost everywhere since  $\frac{\partial^2 L}{\partial \mathbf{s}^2} \succeq 0$  from Lemma A.1.

From above we could see that the Hessian of NNs w.r.t.  $\mathbf{x}$  is at most a rank  $c$  (the number of class) matrix, since the rank of the Hessian matrix

$$\frac{\partial^2 \mathcal{J}(\boldsymbol{\theta}, \mathbf{x}, y)}{\partial \mathbf{x}^2} = \left(\frac{\partial \mathbf{s}}{\partial \mathbf{x}}\right)^T \frac{\partial^2 L}{\partial \mathbf{s}^2} \frac{\partial \mathbf{s}}{\partial \mathbf{x}}$$

is dominated by the term  $\frac{\partial^2 L}{\partial \mathbf{s}^2}$ , which is at most rank  $c$ .

**A.2. Attacks Mentioned in Paper.** In this section, we show the details about the attacks used in our paper. Please see Table 5 for details.

**Table 5:** The definition of all attacks used in the paper. Here  $\mathbf{g}_x \triangleq \frac{\partial \mathcal{J}(\mathbf{x}, \theta)}{\partial \mathbf{x}}$  and  $\mathbf{H}_x \triangleq \frac{\partial^2 \mathcal{J}(\mathbf{x}, \theta)}{\partial \mathbf{x}^2}$ .

	$\Delta \mathbf{x}$
FGSM	$\epsilon \cdot \text{sign}(\mathbf{g}_x)$
FGSM10	$\epsilon \cdot \text{sign}(\mathbf{g}_x)$ (iterate 10 times)
$L_2$ GRAD	$\epsilon \cdot \mathbf{g}_x / \ \mathbf{g}_x\ $
FHSM	$\epsilon \cdot \text{sign}(\mathbf{H}_x^{-1} \mathbf{g}_x)$
$L_2$ HESS	$\epsilon \cdot \mathbf{H}_x^{-1} \mathbf{g}_x / \ \mathbf{H}_x^{-1} \mathbf{g}_x\ $

**A.3. Models Mentioned in Paper.** In this section, we give the details about the NNs used in our paper. For clarification, we omit the ReLU activation here. However, in practice, we implement ReLU regularity. Also, for all convolution layers, we add padding to make sure there is no dimension reduction. We denote Conv(k,k,b) as a convolution layer having b channels with  $k \times k$  filters, MP(k,k) as a  $k \times k$  max-pooling layer, FN(d) as a fully-connected layer with d-dimension output and SM(c) is the soft-max layer with c outputs. For our Conv(5,5,b) (Conv(3,3,b)) layers, the stride is 2 (1). See Table 6 for details of all models used in this paper.

**Table 6:** The definition of all models used in the paper.

Name	Structure
C1 (for CIFAR-10)	Conv(5,5,64) – MP(3,3) – BN–Conv(5,5,64)–MP(3,3)–BN–FN(384)–FN(192)–SM(10)
C2 (for CIFAR-10)	Conv(3,3,63)–BN–Conv(3,3,64)–BN–Conv(3,3,128)–BN–Conv(3,3,128)–BN–FC(256)–FC(256)–SM(10)
C3 (for CIFAR-10)	Conv(3,3,64)–Conv(3,3,64)–Conv(3,3,128)–Conv(3,3,128)–FC(256)–FC(256)–SM(10)
M1 (for MNIST)	Conv(5,5,20)–Conv(5,5,50)–FC(500)–SM(10)
CR (for CIFAR-100)	ResNet20 For CiFar100

**A.4. More Numerical Result for §3.** In this section, we provide more numerical results for §3. All conclusions from the numerical results are consistent with those in §3.

**A.4.1. Results for §3.1 and §3.2.** This section gives extra numerical results for §3.1 and §3.2.

**Table 7:** Result on MNIST dataset for M1 model (LeNet-5). We show the Hessian spectrum of different batch sizes, and the corresponding performance of each model on adversarial dataset generated by training/testing dataset. The results on the test dataset are shown in parenthesis. We report the adversarial accuracy for three different magnitudes of attack denoted by  $\epsilon$ . The interesting observation is that the  $\lambda_1^\theta$  is increasing while the adversarial accuracy is decreasing for fixed  $\epsilon$ .

Batch	Acc	$\lambda_1^\theta$	$\lambda_1^x$	$\ \partial_x \mathcal{J}(\theta, x, y)\ $	Acc $\epsilon = 0.2$	Acc $\epsilon = 0.1$	Acc $\epsilon = 0.05$
64	100 (99.21)	0.49 (2.96)	0.07 (0.41)	0.007 (0.10)	0.53 (0.53)	0.85 (0.85)	0.97 (0.96)
128	100 (99.18)	1.44 (8.10)	0.10 (0.51)	0.009 (0.12)	0.50 (0.51)	0.83 (0.83)	0.96 (0.95)
256	100 (99.04)	2.71 (13.54)	0.09 (0.50)	0.008 (0.12)	0.45 (0.46)	0.81 (0.82)	0.95 (0.95)
512	100 (99.04)	5.84 (26.35)	0.12 (0.52)	0.010 (0.13)	0.42 (0.42)	0.79 (0.80)	0.95 (0.94)
1024	100 (99.05)	21.24 (36.96)	0.25 (0.42)	0.032 (0.11)	0.32 (0.33)	0.73 (0.74)	0.94 (0.94)
2048	100 (98.99)	44.30 (49.36)	0.36 (0.39)	0.075 (0.11)	0.19 (0.19)	0.72 (0.73)	0.94 (0.94)

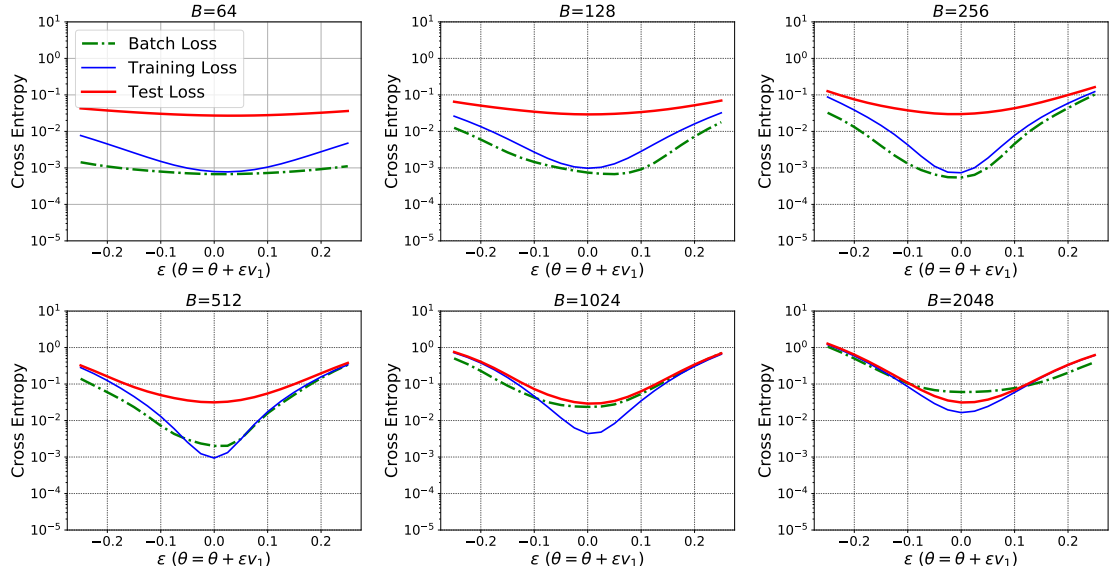


**Fig. 6:** The landscape of the loss functional is shown along the dominant eigenvector of the Hessian for M1 on MNIST. Note that the  $y$ -axis is in logarithm scale. Here  $\epsilon$  is a scalar that perturbs the model parameters along the dominant eigenvector denoted by  $v_1$ . The green line is the loss for a randomly batch with batch-size 320. The blue and red line are the training and test loss, respectively. From the figure we could see that the curvature of test loss is much larger than training.

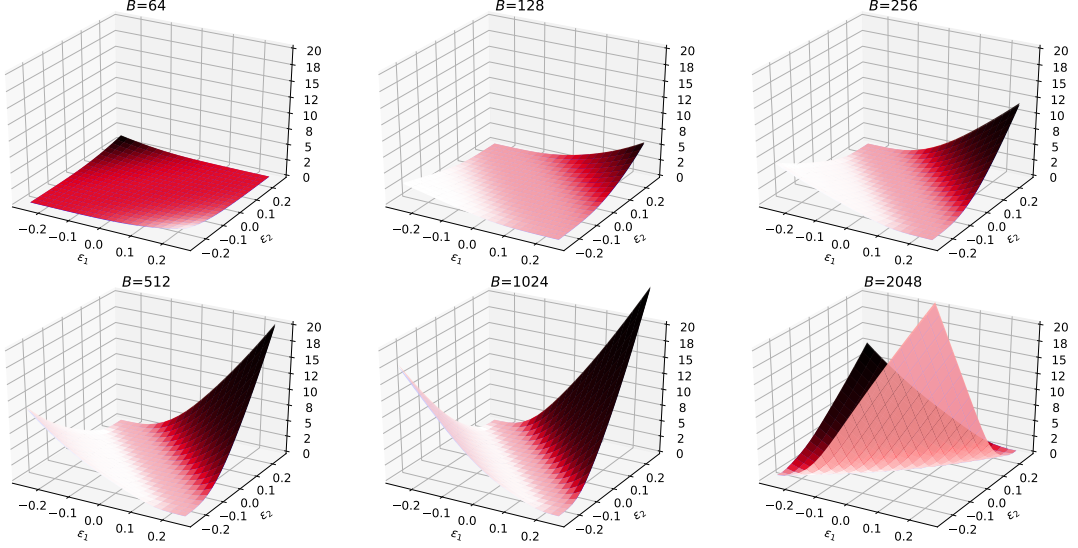


**Fig. 7:** The landscape of the loss functional is shown when the M1 model parameters are changed along the first two dominant eigenvectors of the Hessian. Here  $\epsilon_1$ ,  $\epsilon_2$  are scalars that perturbs the model parameters along the first and second dominant eigenvectors.

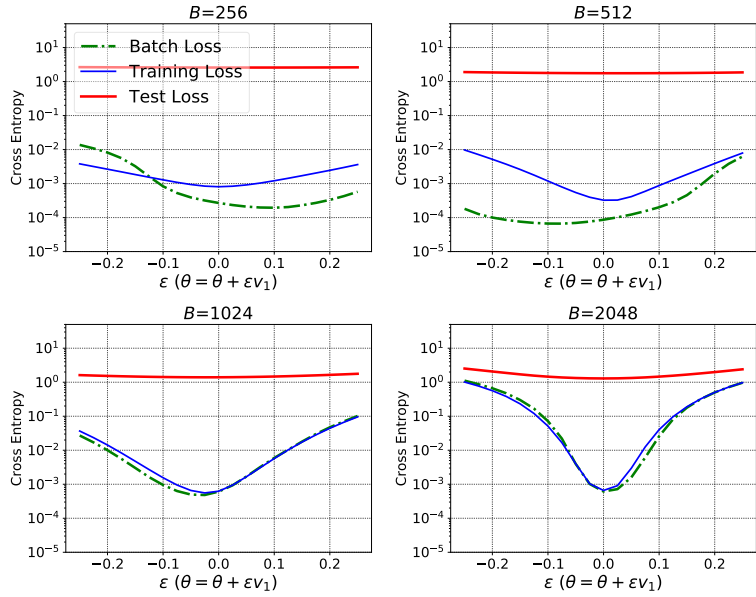


**Fig. 8:** The landscape of the loss functional is shown along the dominant eigenvector of the Hessian for C2 architecture on CIFAR-10 dataset. Here  $\epsilon$  is a scalar that perturbs the model parameters along the dominant eigenvector denoted by  $v_1$ .

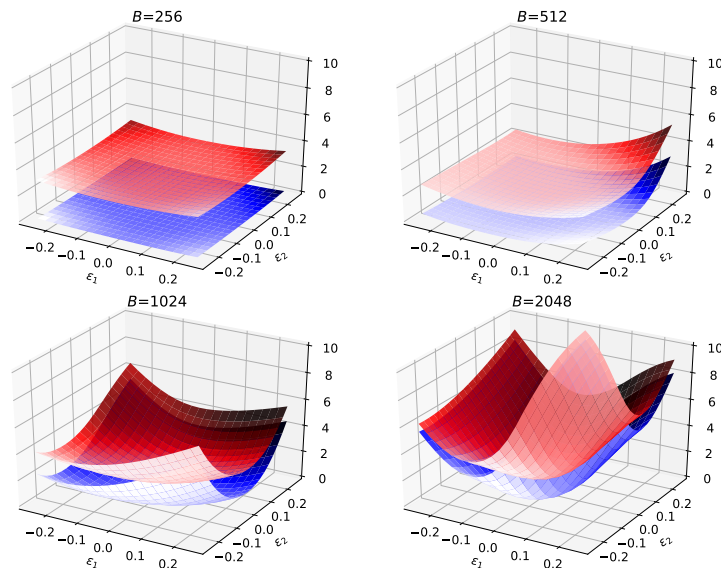


**Fig. 9:** The landscape of the loss functional is shown when the C2 model parameters are changed along the first two dominant eigenvectors of the Hessian. Here  $\epsilon_1$ ,  $\epsilon_2$  are scalars that perturbs the model parameters along the first and second dominant eigenvectors.

**A.4.2. Results for §3.3.** This section gives extra numerical results for §3.3.

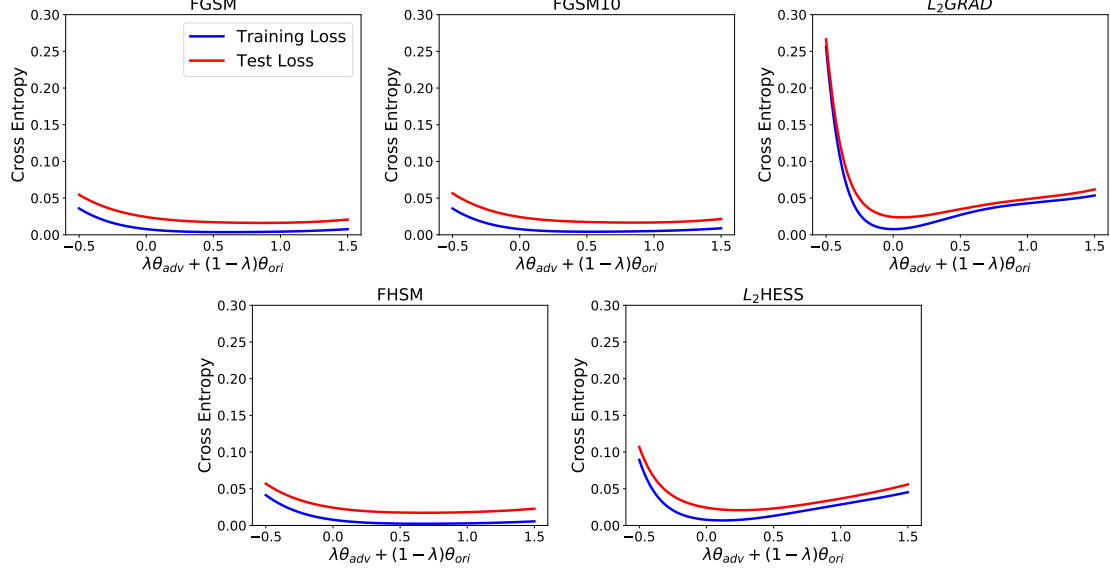


**Fig. 10:** 1-D Parametric Plot for M1 on MNIST of  $\mathcal{M}_{ORI}$  and adversarial models. Here we are showing how the landscape of the total loss functional changes when we interpolate from the original model ( $\lambda = 0$ ) to the robust model ( $\lambda = 1$ ). For all cases the robust model ends up at a point that has relatively smaller curvature compared to the original network.

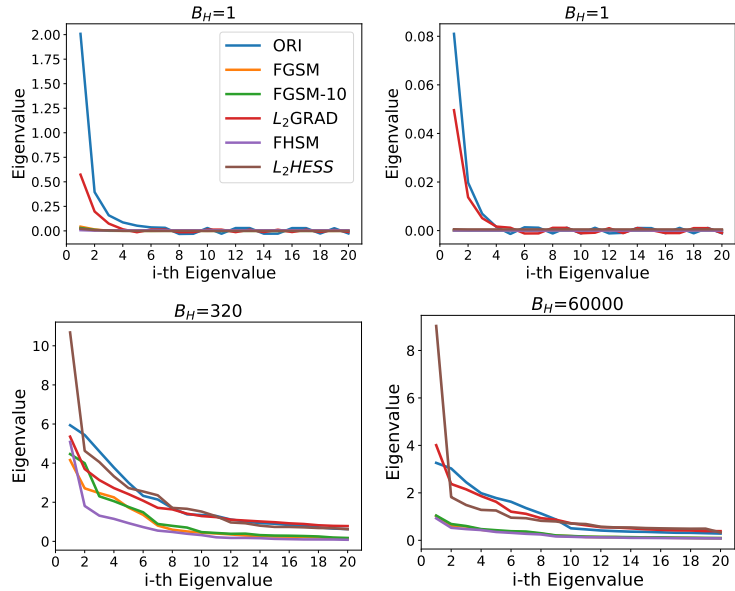


**Fig. 11:** Spectrum of the sub-sampled Hessian of the loss functional w.r.t. the model parameters computed by power iteration of M1 on MNIST. The results are computed for different batch sizes of  $B_H = 1$ ,  $B_H = 320$ , and  $B_H = 60000$ . We report two cases for the single batch experiment, which is drawn randomly from the clean training data. The results show that the sub-sampled Hessian spectrum decreases for robust models. An interesting observation is that for the MNIST dataset, the original model has actually converged to a saddle point, even though it has a good generalization error. Also notice that the results for  $B_H = 320$  and  $B_H = 60,000$  are relatively close, which hints that the curvature for the full Hessian should also be smaller for the robust methods. This is demonstrated in Fig. 12.

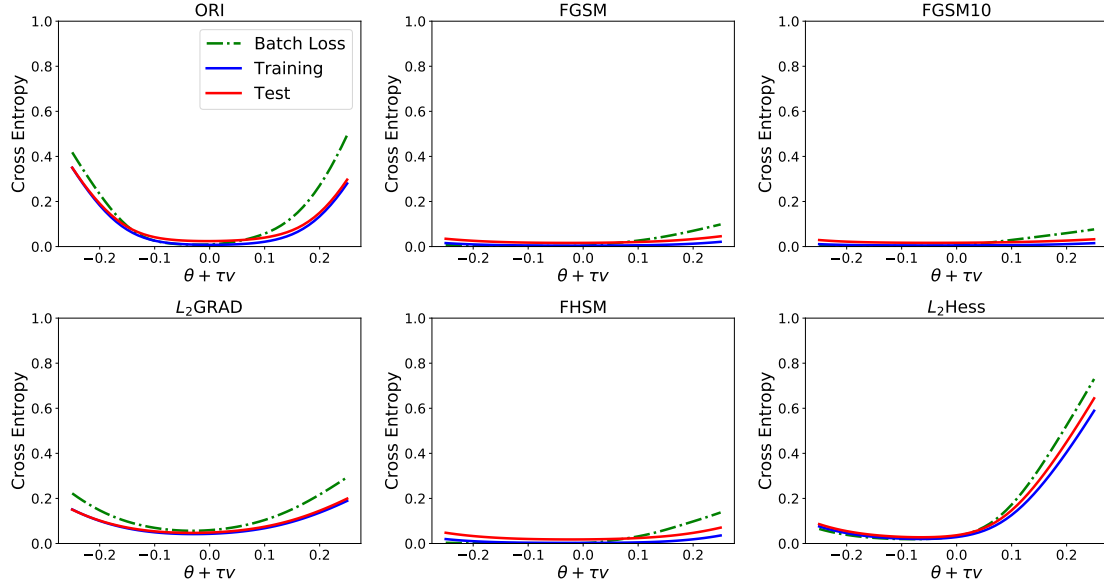


**Fig. 12:** We show the landscape of the test and training objective functional along the first eigenvector of the sub-sampled Hessian with  $B = 320$ , i.e. 320 samples from training dataset, for M1 on MNIST. We plot both the batch loss as well as the total training and test loss. One can see that visually the results show that the robust models converge to a region with smaller curvature.

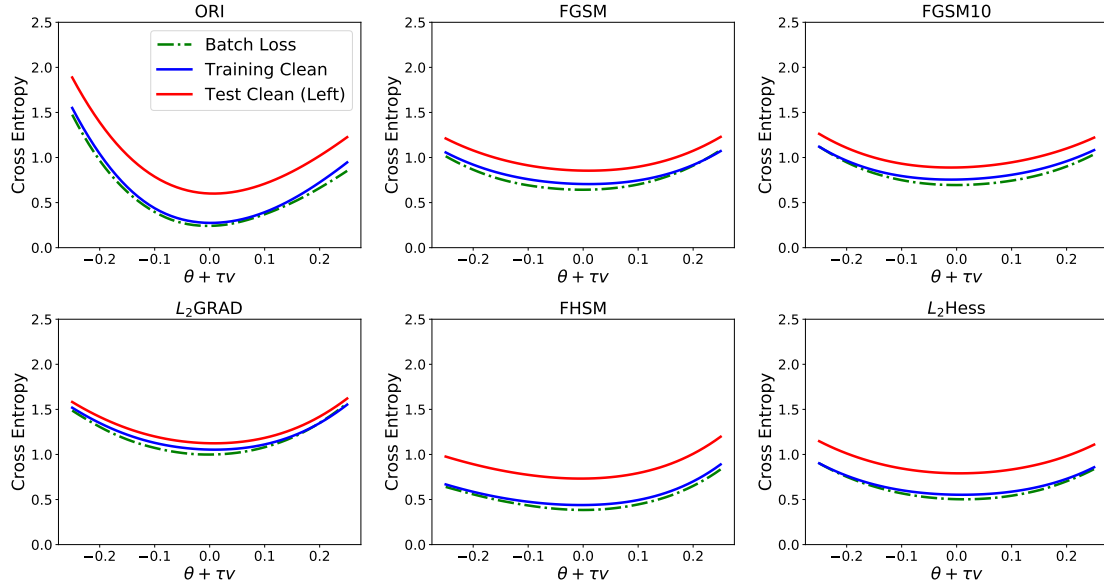


**Fig. 13:** We show the landscape of the test and training objective functional along the first eigenvector of the sub-sampled Hessian with  $B = 320$ , i.e. 320 samples from training, on for C3 on CIFAR-10. We plot both the batch loss as well as the total training and test loss. One can see that visually the results show that the curvature of robust models is smaller.